Int. J. Heat Mass Transfer. Vol. 17, pp. 23–36. Pergamon Press 1974. Printed in Great Britain

RADIATION–CONVECTION INTERACTION IN THE BOUNDARY LAYER REGIME OF AN ENCLOSURE*

J. C. BRATIS and J. L. NOVOTNY

Department of Aerospace and Mechanical Engineering, University of Notre Dame, Notre Dame, Indiana 46556, U.S.A.

(*Received* 17 *January* 1973 *and in revised form* 18 *June* 1973)

Abstract—The interaction of thermal radiation and free convection in the boundary layer regime of a vertical enclosure is analytically and experimentally examined. The local heat flux from the highly-reflecting heated wall in the enclosure is obtained interferometrically; the second wall is a nearly-black cooled plate. The experimental data are compared to a boundary layer type analysis based on the exponential wide-band model. Experiments are presented for pure NH_3, pure N_2, and N_2–NH_3 mixtures for pressures up to 2 bar at a temperature level near 300 K.

NOMENCLATURE

a, dummy variable;
A_{0i}, correlation parameter for ith band;
C^2_{0i}, correlation parameter for ith band;
d_i, $A_{0i}C^2_{0i}e'_{b\omega i}(T_\infty)/M$;
$e'_{b\omega i}$, derivative of the Planck function with respect to temperature;
f, dimensionless stream function;
g, acceleration of gravity;
Gr, Grashof number, see equation (1);
H, height of gas layer;
k, thermal conductivity;
L, thickness of gas layer;
M, $\sum_i A_{0i}C^2_{0i}e'_{b\omega i}(T_\infty)$;
Nu, Nusselt number, see equation (2);
P_a, absorbing gas pressure;
Pr, Prandtl number;
P_t, total pressure;
q, wall heat flux;
q_c, refers to pure conduction or pure convection;
Ra, Rayleigh number;
T, temperature;
x, distance along plate;
y, distance perpendicular to plate;
z, dummy variable;
β, thermal expansion coefficient;
η, dimensionless variable, $y/x(Gr/4)^{\frac{1}{4}}$;
θ, $(T - T_\infty)/(T_w - T_\infty)$ or $(T - T_C)/(Y_H - T_C)$;
ν, kinematic viscosity;
ξ, defined by equation (3);
χ, mole fraction of absorbing gas.

Subscripts

C, cold wall;
H, hot wall;
i, ith band;
w, wall value;
ref, reference level;
∞, free stream value or minimum temperature in boundary layer;
ω, wave number dependent.

* Sponsored by the National Science Foundation under Grant GK 20382.

INTRODUCTION

GASEOUS radiation has been the subject of study by astrophysicists for years but has only received considerable attention by the engineer in the last decade primarily because of hypersonic flight and the reentry process. Obviously, gas radiation is also extremely important in combustion processes that take place in industrial furnaces, internal combustion engines, gas turbines, and jet engines. Interest in pollution and fire prevention has recently accentuated this attention. The primary difficulty in analytically treating gas radiation arises from the complicated nature of the absorption–emission process. Simplified analytical models of absorption bands have to be critically tested against experimental results. In the area of radiation–convection interaction there is a definite lack of experimental data against which analytical models can be compared.

One of the first experimental studies in gaseous radiation interaction was the study by Gille and Goody [1]; this study concentrated on the effect of gaseous radiation on the stability of an horizontal layer heated from below. Other studies in radiation–

conduction interaction are by Schimmel, Novotny and Olsofka [2] and by Olsofka and Novotny [3]. Both employed the same geometry, that of the horizontal layer heated from above. In the area of free convection–radiation interaction there are only the experimental studies by England and Emery [4], and Audunson and Gebhart [5]. England and Emery investigated the effect of thermal radiation upon the boundary layer on a vertical constant heat flux flat plate. Their conclusion was that the effect of gaseous radiation was negligible. Audunson and Gebhart [5] interferometrically studied free convection from a vertical, constant heat flux plate for both absorbing (ammonia) and non-absorbing gases (air, argon). The experiments were conducted for pressures from 2 to 8 bar and for three different plate emissivities. The results presented significant radiation effects and showed trends that are in fair agreement with theoretical predictions based on a gray gas model.

This paper describes an experimental study of radiation–convection interaction in a free-convection boundary layer along a flat plate with emphasis being placed on the examination of the validity of a commonly used non-gray gas model [2, 6]. In this investigation, the free-convection boundary layer is approximated experimentally by the boundary layer regime in a rectangular enclosure. The two bounding vertical plates in the enclosure are at constant but different temperatures. The heated plate has a reflectivity close to one while the other plate has a reflectivity of nearly zero. As has been discussed elsewhere [7, 8], there exist, basically, three laminar flow regimes in the enclosed layer depending on the value of the Rayleigh number, the Prandtl number, and the aspect ratio. For small values of the Rayleigh number the heat is transferred mainly by conduction although there is a small unicellular motion in the fluid. At large values of the Rayleigh number there are two boundary layers formed at the walls resembling the boundary layer formed on a vertical heated or cooled plate in an infinite medium with the exception of the corner regions. For intermediate values of the Rayleigh number, there exists a transitional regime between the conduction and the boundary layer regime. The experiments are run for two values of the aspect ratio such that results can be obtained for the conduction and the boundary layer regimes.

Nitrogen, ammonia, and their mixtures at different pressures and mole fractions are employed in this study. Temperature profiles across the layer and local wall heat fluxes are obtained interferometrically. The experimental results for pure nitrogen are used as a reference base for the comparison of the ammonia local heat flux results with an analytical solution based on the non-gray exponential wide-band model [6, 9]. The exponential wide-band model has proven to be successful in predicting radiation–conduction interaction in horizontal gas layers [2, 3]; the radiation–convection interaction analysis used here is based on the investigation of Bratis and Novotny [6].

DESCRIPTION OF EXPERIMENTAL APPARATUS AND PROCEDURE

The two vertical plates used in the present investigation were constructed by Schimmel [10]. The 50·8 cm by 50·8 cm plates were manufactured from 6061-T651 aluminum tooling plate. The plates were instrumented with a sufficient number of thermocouples for monitoring the temperature. One of the plates was heated by four strip heaters epoxied on its back side; the other plate was maintained at room temperature by circulating water from a constant temperature bath through cooling channels. To enhance interaction effects and to simulate a free convection boundary layer in an infinite environment, the cool plate was coated with 3M Nextel black velvet paint to decrease its emittance. Based on the manufacturers

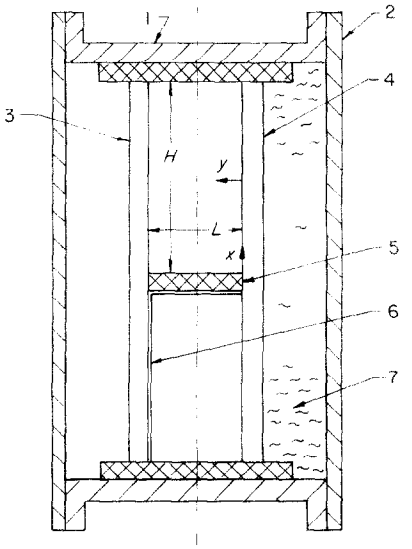

1 Pressure chamber
2 Cover plate
3 Cold plate
4 Heated plate
5 Neoprene foam
6 Aluminum sheet
7 Cotton used as insulator

FIG. 1. Schematic of apparatus.

specifications and an experimental check, the reflectivity is less than 0·03. The highly-reflecting heated plate was the same plate used in [2]; the reflectance characteristics remained the same as those quoted in [2].

The two vertical plates were enclosed in a pressure chamber with inside dimensions 55·9 cm by 55·0 cm and 35·5 cm wide. It was constructed by welding 6061-T651 aluminum tooling plate; with the two 55·9 cm by 55·9 cm sides open. A flange having an O-ring groove was welded on each of the open sides; the chamber could be easily sealed by two aluminum cover plates. A schematic section of the apparatus perpendicular to the light beam direction is given in Fig. 1. Figure 1 represents the configuration used in the small aspect ratio experiments. Two pairs of viewing ports were installed on the other two sides of the chamber in order to allow passage of the interferometer beam. The ports were positioned such that a large portion of the slot height could be viewed by either raising the apparatus or turning the apparatus upside down. The ports were pressure sealed with optical flats 1·9 cm thick held by aluminum rings or aluminum cover plates depending on the mode of operation. The thick optical flats were separated from the heated gas layer by Brewster windows (2 mm thick) held in place by Plexiglas holders.

Figure 2 presents a photograph of the pressure chamber without one of the large cover plates. Inside the chamber, the back of the heated plate is shown; the horizontal stripes are the strip heaters covered with epoxy. In order to apply the required voltage on the strip heaters from the outside of the pressure chamber, the copper buss bars at the end of each strip were connected through lead wires to another set of buss bars epoxied to an O-ring sealed plug. These plugs are visible in Fig. 2 together with the buss bars. Similar plugs were used for bringing the thermocouple wires out of the pressure chamber.

The spacing between the vertical plates was dictated by four micarta plugs positioned at the corners of the plates. The spacings used in the experiments were 1·78 cm and 6·35 cm. With the 1·78 cm spacing, the entire height of the slot was used giving an aspect ratio (height/spacing) of 28. With the 6·35 cm spacing, only half of the height of the slot was used (separated from the rest of the slot by neoprene foam) giving an aspect ratio of 4 (see Fig. 1). The

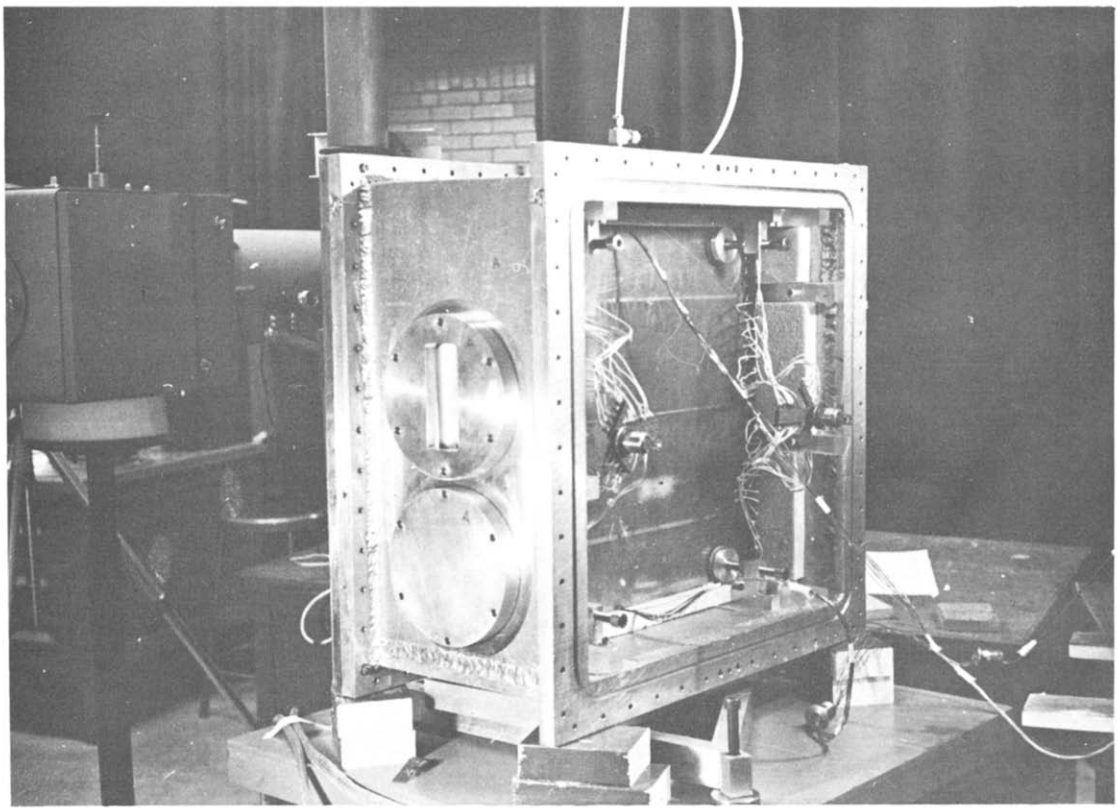

FIG. 2. Photograph of apparatus.

plates were kept approximately 2·5 cm away from the walls of the pressure chamber by use of Plexiglas bars in order to avoid excessive heat losses. Except for small viewing slots, the edges of the gas layer were bounded with open-cell neoprene foam.

The copper–constantan thermocouples used for obtaining the plate temperatures were calibrated with a Leeds and Northup six dial potentiometer against a National Bureau of Standards calibrated resistance thermometer. During the experiments the thermocouples output was monitored with a digital potentiometer (Honeywell, Model 40011-20/21). Cooling water was supplied to the cool plate by a Brinkmann–Lauda bath with a rated control accuracy of $\pm 0{\cdot}03$ K.

The Mach–Zehnder interferometer was manufactured by Intertech Corporation and has 15·2 cm optics. The plates were aligned vertically using a plumb line as reference. The method described by Howes and Buchele [11] was used for aligning the plates parallel to the light beam.

The gases employed in the experiments were nitrogen, ammonia and nitrogen–ammonia mixtures. The nitrogen was the Matheson prepurified grade; the anhydrous ammonia, also obtained from Matheson Company, was better than 99·95 per cent pure according to specifications. For the experiments with pure nitrogen and pure ammonia the pressure chamber was evacuated and then filled with the appropriate gas at least twice, in order to insure a purity well above 99 per cent. In the conduction regime mixture runs, the pressure chamber was filled first with nitrogen and then with ammonia: the mole fraction was specified by monitoring the pressure in the chamber with two calibrated Heise gages. A sufficient time period was allowed to insure proper mixing of the gases. To conserve time in the convection runs, a mixing tank was utilized.

At the start of an experimental run, an interferogram was taken with the fringes horizontal. A voltage was applied across the strip heaters and the constant-temperature bath was activated with its temperature level set at the desired temperature (room temperature) of the cold plate. When the desired temperature difference between the two plates was reached, the voltage across the heaters was reduced. If the temperature readings did not change more than $\pm 3\,\mu$V in a period of 20 min, quasi-steady state was assumed and a final interferogram was recorded. In the small-spacing runs, the fringes were rotated before a final interferogram was taken. This accentuated the wall derivatives of the fringe profile as noted by Schimmel, Novotny and Osolfka [2]. In the runs with the large

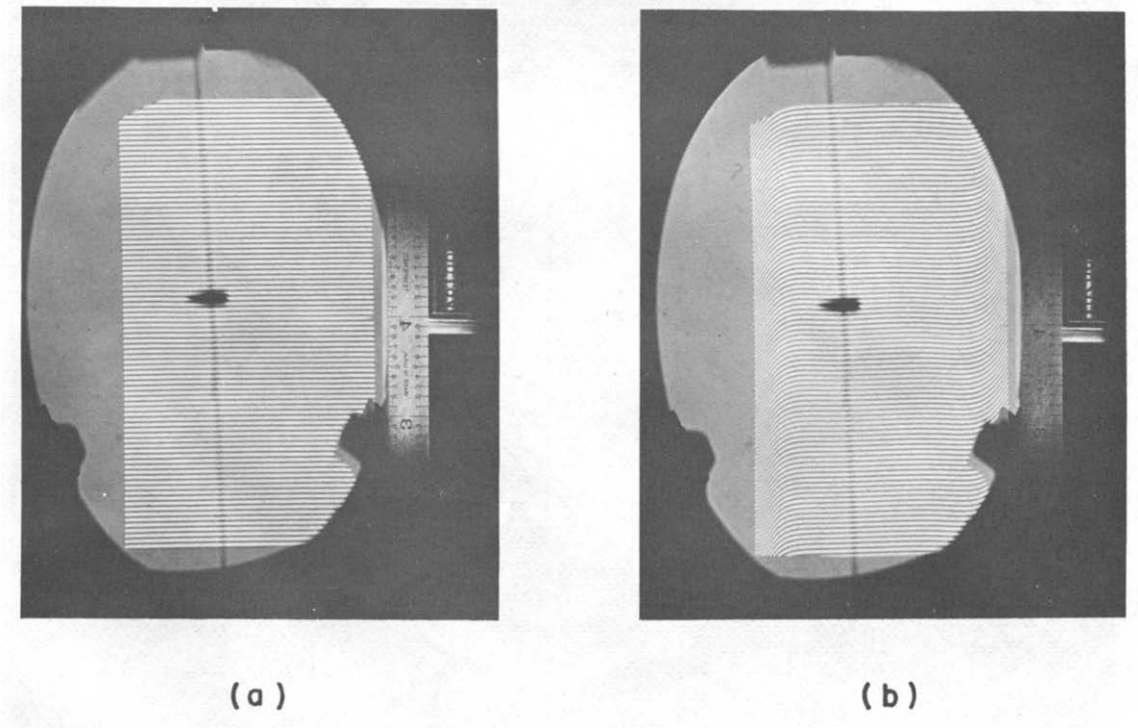

FIG. 3. Sample interferograms: $H/L = 4$, $L = 6{\cdot}35$ cm, $P_t = 2$ bar, $\chi = 0{\cdot}75\ T_{ref} \approx 300$ K. (a) initial, $\Delta T = 0$ K; (b) final, $\Delta T = 7$ K.

spacing, the fringes were not rotated. The interferograms were taken on Kodak Royal Pan 4 × 5 film using a Super Speed Graphic camera without a lens.

To conserve space only a brief description of the interferogram analysis will be given here. In this type of system, a reference temperature is not available. To offset this difficulty, the measured temperature difference between the plates was used to calculate the total fringe shift across the gas layer. This value was then used as a basis to correct the data obtained from the fringe pattern. Optical imperfections in the system were too small to warrant correction by using the initial fringe pattern. Examples of an initial fringe pattern and a final fringe pattern for the large aspect ratio case are given in Fig. 3. All interferograms were analyzed on a Gaertner model M2001 toolmakers microscope. By examination of the repeatability of the data from a number of interferograms, it was determined that the fringe profiles could be obtained to better than $\pm\frac{1}{30}$ fringe. This, of course is not true very near the wall; the procedures used for extrapolation to the wall are discussed in [10, 14]. The Gladstone–Dale approximation to the Lorenz-Lorentz equation was employed in the interferogram analysis; the principle of additivity for the molar refractivity was used in the mixture runs. The nitrogen and ammonia properties necessary for evaluating the Gladstone–Dale constant were obtained from [12, 13], respectively; the densities were evaluated from the perfect gas law. Since the pressures in the experiments were limited to 2 bar or less, the compressibility error due to using the perfect gas law for NH_3 is about 2 per cent at the temperature level of the experiments. In light of other property uncertainties, it is felt that the use of the perfect gas law is justified.

Length limitations allowed only a brief discussion of the experimental apparatus, experimental procedure, data reduction and errors to be presented here; a detailed discussion of these points can be found in [14]. Examples of prior interferometric work using similar procedures can be found in [2, 3, 10].

RESULTS AND DISCUSSION

Conduction regime

Data for the conduction regime were obtained from the experimental runs with the small spacing of the plates. Data for the boundary layer regime could not be obtained with this spacing because the flow would become unstable before reaching the boundary layer regime. The presence of instabilities resulted in fluctuations of the fringe pattern, resembling wave motion. The onset of the instabilities was difficult to detect because the fronge motion could only be detected on the ground glass of the camera when the amplitude of the fringe fluctuations became larger than about 0·3 of the fringe spacing. The lower value of the Rayleigh number at which instabilities were observed for the small spacing and the large aspect ratio ($H/L = 28$) was $0{\cdot}7 \times 10^4$. This value is in satisfactory agreement with the value presented by Gill and Davey [15] which is $0{\cdot}65 \times 10^4$.

The heat transfer result for the conduction regime

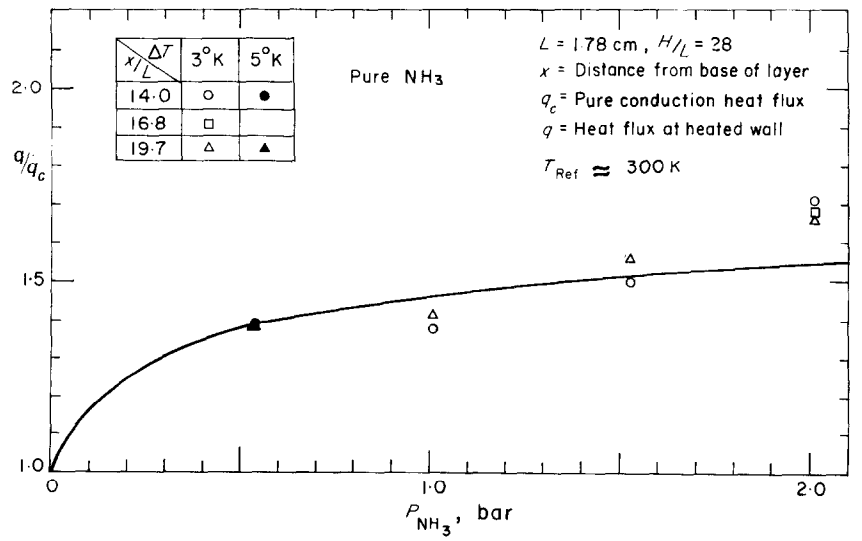

FIG. 4. Effect of radiation interaction; conduction regime.

are presented as a ratio of the heat flux at the heated wall to that for pure conduction. Figure 4 presents the results for pure ammonia. The lines in the graph represents an analytical solution obtained with the method given by Schimmel, Novotny and Olsofka [2] and Schimmel, Novotny and Kast [16]. The analytical solution, based on linearized radiation, utilizes the exponental kernel approximation and the correlation for the total band absorptance given by Tien and Lowder [17]. For the present case the reflectance of the heated wall was taken equal to 0·95* and that of the cold wall equal to 0·05. It should be noted that the analysis is based on diffuse surfaces. The introduction of a specular boundary condition would have little effect on the final results presented here [16]. The spectroscopic constants of ammonia were taken from [6]. The experimental results for pure NH_3 were obtained for a temperature difference of 3 K, except for the data corresponding to 0·5 bar which were obtained for a temperature of 5 K: this larger temperature difference increased the accuracy of the interferogram analysis by increasing the total fringe shift.

The agreement between the experimental results and the analytical solutions is good except at 2 bar. The discrepancy at 2 bar between the data and the analytical results are interpreted to be caused by convection: pure N_2 data, which are not given here, support this conclusion. The presence of free convection is also in agreement with the results of Eckert and Carlson [7]. From their results, one finds that for a Grashof number, based on the width of the layer, of the order 10^4 (which is the order of the Grashof number for the runs with a total pressure of 2 bar) the enclosed layer is in the transition regime.

Although the primary emphasis of this paper is the boundary layer regime, the previous results were presented to verify the values of the spectroscopic constants [6] and the proper behavior of the experimental apparatus. Additionally, the conduction–radiation interaction results are for the nearly black wall and one highly reflecting wall which differs from the two highly reflecting wall case previously studied [2]; these results support the conclusion of [2] that the exponential wide-band model is the correct model for predicting radiation–conduction interaction.

Boundary layer regime

Data in the boundary layer regime were obtained from the experiments with the spacing $L = 6{\cdot}35$ cm and an aspect ratio of $H/L = 4$. Values in the conduction regime for this aspect ratio could not be obtained because free convection was present even for small values of the temperature difference. For large values of the Rayleigh number, instabilities were noticed by the presence of wave motion in the fringe pattern. The minimum value of the Rayleigh number for which instabilities were observed was $Ra_L = 6{\cdot}8 \times 10^5$. This value is in good agreement with the one predicted (7×10^5) by Gill and Davey [15]. For runs in the boundary layer regime in which wave motion was observed, the fluctuation of the fringes had a small amplitude and therefore the influence on the temperature profile was very small. The influence of the fluctuations on the estimation of the temperature wall gradient was negligible: the fluctuations were more or less confined in the core region of the layer.

Figure 3 presents two of the interferograms taken during the experimental run with a mixture of ammonia and nitrogen at a total pressure of 2 bar, the mole-fraction of ammonia being $\chi = 0{\cdot}75$. The initial interferogram with zero temperature difference between the plates is given in part (a) of Fig. 3. Only a small portion of the cold wall, which is on the right, appears in the interferogram. This was done in order to obtain the maximum portion of the heated wall in the interferogram: the study was centered on the heat transfer from the highly-reflecting wall.* The narrow black shadow from a needle indicates the height of 15·7 cm measured from the bottom of the enclosure. The top of the layer is towards the top of the page. Figure 3 (b) is the interferogram taken with a temperature difference of 7 K. The fringes in the center region of the layer are nearly horizintal indicating an approximately constant temperature across the layer. Close to the walls the fringes are bent indicating a temperature gradient perpendicular to the walls and therefore a boundary layer along each wall. The corresponding value of the Rayleigh number is $Ra_L = 8{\cdot}15 \times 10^5$. Although this is larger than the minimum Ra_L for which instabilities have been noticed ($6{\cdot}8 \times 10^5$), the fringe pattern did not exhibit detectable fluctuations. The results presented in this study correspond to situations where fluctuations were absent from the interferograms: it should be pointed out that characteristics of strong second-

* Due to a programming error, this value is slightly higher than the measured value [2]. Since the wall temperature gradients are insensitive to the reflectance for reflectances near one [16], the error in the analysis given in Fig. 4 is less than 2 per cent.

* Under perfectly-reflecting conditions, the total heat flux at this wall would be the conductive flux.

ary flows as noted by Elder [8] were absent from the data.

The temperature distribution along the vertical in the mid-plane between cold and heated wall is presented in Fig. 5 for four different pressures. The temperature is plotted in a dimensionless form versus the dimensionless height of the gas layer. The open circles correspond to values obtained with pure nitrogen and the closed circles to values obtained with pure ammonia. All data were obtained with a temperature difference of 7 K except the data for 0·5 bar which were for a temperature difference of 8 K. The centerline temperature distribution obtained for nitrogen is in good agreement with the results of Eckert and Carlson [7]. It is seen that in all cases the centerline temperatures for ammonia are consistently lower than the corresponding temperatures for nitrogen. The heated wall has an emittance of nearly zero while the cold wall has an emittance close to one. It is, therefore, reasonable to expect that in the case of ammonia, heat is transferred by radiation from the gas to the cold wall resulting in a lower centerline temperature than in the pure nitrogen case. Results for NH_3–N_2 mixtures at total pressures of 1 and 2 bar exhibit basically the same behavior [14]; to conserve space, they were omitted here.

The temperature profile across the layer at a height of 15 cm is presented in Fig. 6 for pure NH_3 and pure N_2 at total pressures of 1 and 2 bar. It is seen from Fig. 6 that the temperature gradient at the heated highly-reflecting wall for pure NH_3 is greater than that for pure N_2 at both total pressures. The temperature gradient at the nearly-black cold wall has a different behavior. At a pressure of 1 bar the temperature gradient at the cold black wall for NH_3 is less than that for N_2; at a pressure of 2 bar, the temperature gradient exceeds the value of the gradient for pure nitrogen. This behavior* agrees with the behavior of the conductive heat flux found

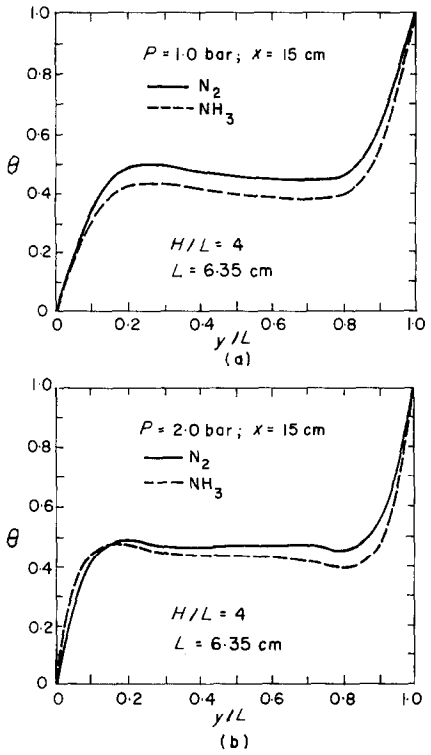

FIG. 6. Experimental temperature profiles; boundary-layer regime.

* A similar behavior was found in the NH_3–N_2 mixture results. The variation of the gradient at the cold wall with pressure is related to the ability of the gas to directly exchange energy by radiation with the nearly-black cold wall.

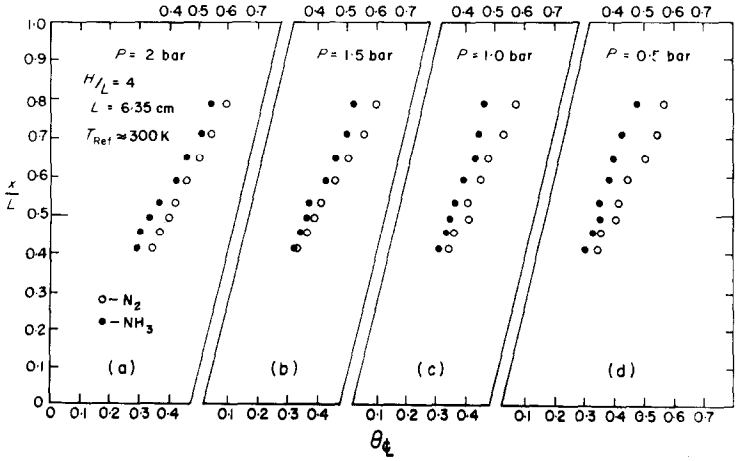

FIG. 5. Centerline temperature distribution.

by Schimmel, Novotny and Kast [16] in a radiation–conduction interaction situation. The reverse temperature gradient in the core of the layer is characteristic of the boundary layer regime in an enclosure [8, 18]. The slight bumps in the profiles near $y/L = 0{\cdot}2$ and $0{\cdot}8$ are partially caused by optical imperfections which are more apparent at the higher pressures; these also might be indicative of the onset of secondary flow, however, all other characteristics of a strong secondary flow are missing [8].

Eckert and Carlson [7] succeeded in correlating their data from the rectangular enclosure by plotting them as the local Nusselt number versus the local Grashof number. For a characteristic temperature difference, they employed the difference between wall and centerline temperature. As was mentioned in the discussion of Fig. 6, the presence of an absorbing-emitting gas, combined with the asymmetric radiative boundary conditions, significantly affects the centerline temperature.* For this reason, in this investigation, the temperature difference was chosen as the difference between the wall temperature, T_w, and the temperature at which the temperature gradient becomes zero as one moves away from the wall, T_∞. The local Grashof and Nusselt numbers are then given by:

$$Gr = g\beta(T_w - T_\infty)x^3/\nu^2 \tag{1}$$

$$Nu = qx/(T_w - T_\infty)k \tag{2}$$

where x denotes the distance from the starting corner of the plate (the base of the enclosure). The temperature T_∞ was obtained by plotting the temperature profile across the layer. Figure 7 presents examples of the experimental temperature profiles for pure ammonia and pure nitrogen at 2 bar for different heights in the layer. It should be noted that only for the height of 15 cm. was the interferogram analyzed across the whole layer; for all other heights, the interferograms were analyzed from $y/L = 0{\cdot}4$ to $y/L = 1{\cdot}0$.

The local heat transfer results obtained from the experiments are presented as the Nusselt number versus the Grashof number as defined in equations (1) and (2). The results for pure nitrogen are presented in Fig. 8 for four pressures. The solid line represents the best fit to the data of Eckert and Carlson [7]; the dashed line represented the solution for laminar free convection from a vertical constant-temperature

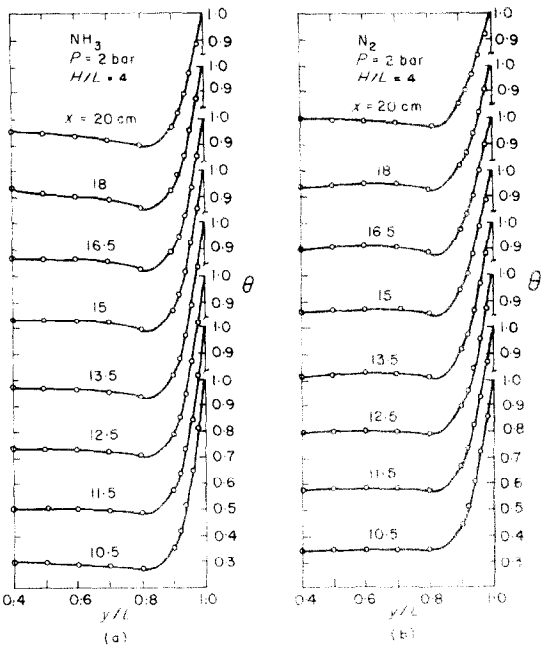

FIG. 7. Experimental temperature profiles: boundary-layer regime.

plate. The results for each pressure level can be approximated by a straight line having about the same slope as the slope of the Eckert and Carlson line. It is noticed, however, that the magnitude of the Nusselt number decreases with increasing pressure level. It is felt that this effect is real and not the result of inaccuracies in the data. This behavior suggests that the growth of the boundary layer is approximately the same for all pressures but that the pressure possibly has an effect on the turning behavior of the flow in the corners resulting in a different characteristic starting length x/L for each pressure. This conclusion is pure speculation but the authors find no other explanation of the pressure behavior.

The experimental data for pure ammonia and ammonia–nitrogen mixtures are presented in the same manner as the pure nitrogen data. Figure 9 shows the results obtained for pure ammonia at pressure of 1·5 and 2 bar. The open circles indicate the N_2 data presented in Fig. 8; the solid line averages the nitrogen data points. The dark points indicate the ammonia data. The dashed line represents the theoretical prediction based on the results of Bratis and Novotny [6]. This analysis [6], which is based on a perfectly reflecting wall* with a black wall at

* This is also clear from the mixture profiles given in [14]. It should be re-emphasized that only the gradient at the highly-reflecting heated wall will be treated in the comparisons presented here.

* This approximates the experimental reflectance ($\approx 0{\cdot}91$ in the region of the strong NH_3 band [2]); however the wall temperature gradients should be insensitive to the reflectance for reflectances near one [5, 16].

the free-stream temperature located outside the boundary layer, employs series expansions for the dimensionless stream function and temperature in terms of a parameter representing the relative role of radiation to convection. This parameter is defined as

$$\zeta = \frac{P_a x^2}{kGr^{\frac{1}{4}}} \sum_i A_{0i} C_{0i}^2 e'_{b\omega i}(T_\infty) \tag{3}$$

where $A_{0i}C_{0i}^2$ is the band intensity of the ith band, and $e'_{b\omega i}(T_\infty)$ is the derivative of the Planck function evaluated at the free stream temperature and at the center of the ith band. This parameter is commonly encountered in radiation–convection problems, for example see [19].

Using the approximations necessary to formulate the radiative term in the energy equation in terms of the total band absorption [2, 6, 16, 19], the non-gray exponential wide-band model for the total band absorption was used in the limits of high and low pressure.* This finally results in two sets of approximate ordinary differential equations where for high pressures the band absorption is represented by a logarithmic behavior and at low pressures by a square-root behavior.*

To serve as an example to the reader, the final equations for the logarithmic region will be reproduced here. The stream function and temperature expansions for this region take the form

$$f(\xi, \eta) = f_0(\eta) + f_1(\eta)\xi^{\frac{1}{2}} + f_2(\eta)\xi + \ldots \tag{4}$$

$$\theta(\xi, \eta) = \theta_0(\eta) + \theta_1(\eta)\xi^{\frac{1}{2}} + \theta_2(\eta)\xi + \ldots \tag{5}$$

Following procedures previously used [2, 16] and invoking the logarithmic approximation for the total band absorption, the conservation equations yield the following set of ordinary differential equations for ξ^0

$$f_0''' + 3f_0 f_0'' - 2(f_0')^2 + \theta_0 = 0 \tag{6}$$

$$\frac{1}{Pr}\theta_0'' + 3f_0\theta_0' = 0 \tag{7}$$

for $\xi^{\frac{1}{4}}$

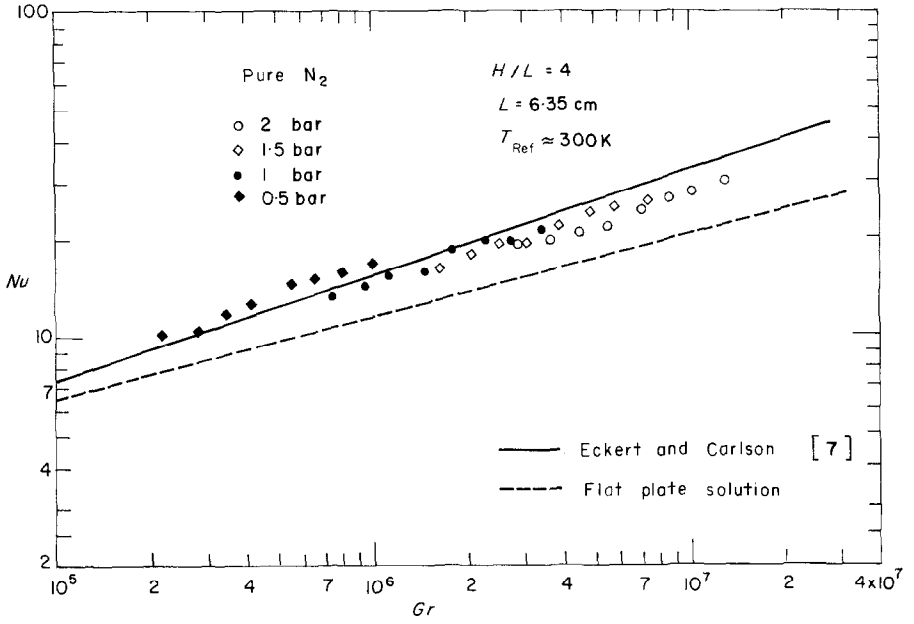

FIG. 8. Heat transfer for pure N_2; boundary-layer regime.

* One should differentiate between pure NH_3 and pressure broadened NH_3 (N_2–NH_3 mixtures); however, in both cases, the total pressure governs the region of the total band absorption required for the heat transfer calculations [6].

* The linear region for the total band absorption does not apply in the range of pressures considered here [6]. It should be noted that this approach assumes that the boundary layer is entirely within the square-root absorption region or the logarithmic absorption region.

$$f_1''' + 3f_0f_1'' - 5f_0'f_1' + 4f_0''f_1 + \theta_1 = 0 \quad (8)$$

$$\frac{1}{Pr}\theta_1'' + 3f_0\theta_1' - f_0'\theta_1' + 4f_1\theta_0' = \frac{2}{Pr}\left(\frac{M}{2kP_a}\right)^{\frac{1}{2}} \sum_i \frac{d_i}{C_{0i}^2} L_i(\theta_0') \quad (9)$$

for ξ

$$f_2''' + 3f_0f_2'' - 6f_0'f_2' + 5f_0''f_2 + 4f_1f_1'' - 3(f_1')^2 + \theta_2 = 0 \quad (10)$$

$$\frac{1}{Pr}\theta_2'' + 3f_0\theta_2' - 2f_0'\theta_2 + 4f_1\theta_1' - f_1'\theta_1 + 5f_2\theta_0' = \frac{2}{Pr}\left(\frac{M}{2kP_a}\right)^{\frac{1}{2}} \sum_i \frac{d_i}{C_{0i}^2} L_i(\theta_1') \quad (11)$$

where

$$L_i(a) = \int_0^{\eta} \tilde{e}_i \frac{a\,dz}{\eta - z} - \int_{\eta}^{\infty} \tilde{e}_i \frac{a\,dz}{z - \eta} - \int_0^{\infty} \tilde{e}_i \frac{a\,dz}{\eta + z} \quad (12)$$

and $\tilde{e}_i = 1{\cdot}0$ for linearized radiation. The boundary conditions are given by

$$\eta = 0: \quad f_0 = f_1 = f_2 = \ldots = 0$$
$$f_0' = f_1' = f_2' = \ldots = 0$$
$$\theta_0 = 1, \theta_1 = \theta_2 = \ldots = 0$$
$$\eta \to \infty: \quad f_0' = f_1' = f_2' = \ldots = 0$$
$$\theta_0 = \theta_1 = \theta_2 = \ldots = 0.$$

Sample analytical results for pure NH_3 are given in Fig. 10; the results for N_2–NH_3 mixtures exhibit the same basic behavior. The reader is referred to reference [6] for a detailed development and discussion of the analysis; the property values (spectroscopic and transport) necessary for the results presented here are also given in [6].*

The analytical predictions represented by the dashed lines in Fig. 9 are obtained from results similar to those shown in Fig. 10. Since the numerical solutions of the non-radiating enclosure problem are rather limited, the predictions for the radiating case must use the N_2 data as a base. To accomplish, this, one must take into account the variation due to the difference in the Prandtl number between pure NH_3 and pure N_2 (0·91 for NH_3 as compared to 0·71 for N_2 at 300 K). Without additional information, it was necessary to assume that the Prandtl number effect in the enclosure is the same as that for a constant temperature vertical flat plate. This is then combined with the increase in heat flux due to gaseous radiation as predicted from results such as those shown in Fig. 10 for each corresponding ξ value and pressure. The combination of these two effects predicts a value of the Nusselt number at a given Grashof number for NH_3; this is shown as the dashed lines on Fig. 9.

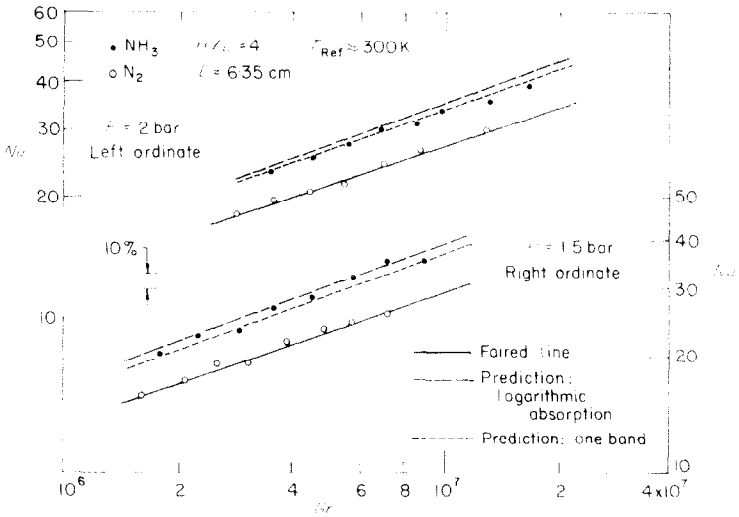

FIG. 9. Effect of radiation interaction for pure NH_3; boundary-layer regime.

* For the small temperature differences encountered in the experiments, all analytical results are based on linearized radiation. It should be noted that the data of [5] indicate an increasing interaction with pressure at $P \approx 6$ bar whereas the results in Fig. 10 indicate a decreasing interaction at this pressure level; this is probably due to the difference in the boundary conditions.

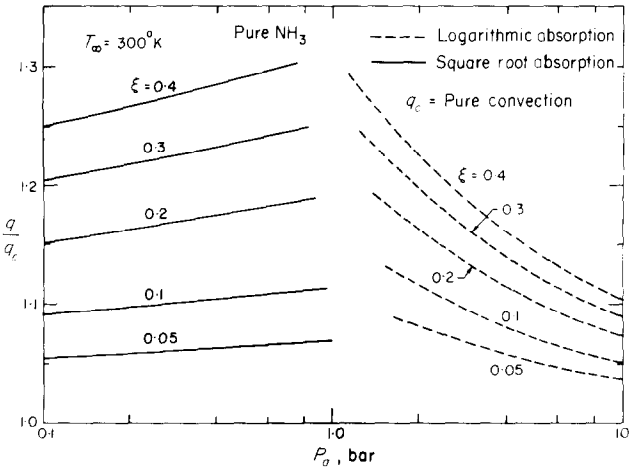

FIG. 10. Analytical results for radiation interaction in a free-convection boundary layer [6].

As presented in Fig. 5 and discussed by Eichhorn [20], the thermal stratification in the core of the enclosure influences the local heat transfer rates for non-radiating gases. This effect is approximately taken into account since the radiating gas results are based on the nitrogen data; however, it should be noted that the effect of gaseous radiation on the local heat-transfer rates is estimated using a local temperature difference. The effect of using a local temperature difference for estimating the magnitude of interaction should introduce little error into the final results since the correction due to the interaction itself is fairly small.

The agreement between the analytical predictions and the pure NH_3 data for 2 bar and 1·5 bar is excellent as shown in Fig. 9. The predictions at this pressure level use the logarithmic limit (see Fig. 10). The two NH_3 absorption bands which play a role at this temperature level are the 950 and 1627 cm^{-1} bands; the strongest of the absorption bands (950 cm^{-1}) dictates the absorption region used in the analysis. This, of course, has a tendency of overestimating the effect of the weaker band. To determine the magnitude of this effect, two analyses were completed, one with both bands and one with only the strong band; the effect of the weak band is very small as shown in Fig. 9 (the difference between the two dashed lines). At the pressures given in Fig. 9, the agreement between theory and experimental is excellent.

Figure 11 presents similar information for pure NH_3 at pressures of 0·5 and 1 bar. The analytical

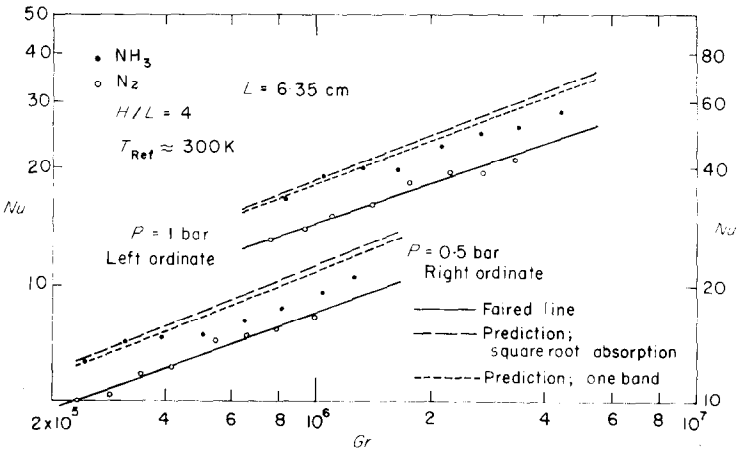

FIG. 11. Effect of radiation interaction for pure NH_3; boundary-layer regime.

predictions at these pressures are based on the square-root absorption region. The agreement between the data and the analysis is not as good as the prior cases. The lack of agreement, especially at the higher Grashof numbers, can be due to a number of reasons. Figure 10 shows that the analytical prediction is between the square-root and logarithmic regions. Additionally, the heated boundary layer turning region encompasses a space approaching $H/2$ [21] in the upper portion of the enclosure. As the pressure decreases, this turning region could increase due to boundary layer growth; gaseous radiation effects also have a tendency to increase the boundary layer thickness. Two dimensional radiation effects could

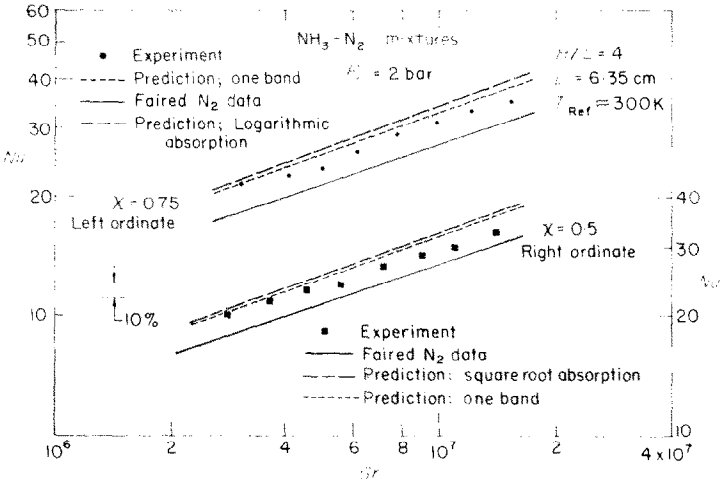

FIG. 12. Effect of radiation interaction for N_2–NH_3 mixtures; boundary layer regime, $P_t = 2$ bar.

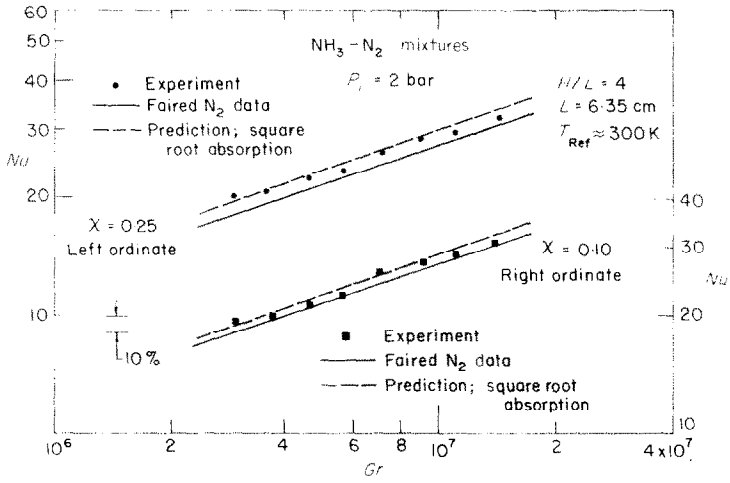

FIG. 13. Effect of radiation interaction for N_2–NH_3 mixtures; boundary layer regime, $P_t = 2$ bar.

If one assumed a smooth transition between the limits, the use of the logarithmic or square-root results for the intermediate region will have a tendency of overestimating the data. The analysis is based on a perfectly reflecting wall; this would also have a tendency of overestimating the interaction effects. also influence the experimental results. Finally, the analysis is approximate in the sense that it represents a boundary layer as completely in the square-root absorption region or the logarithmic region. This approximation is poor for the square-root region since in addition to the linear behavior of the

absorption near the wall there is always an outer region of the boundary layer in the logarithmic limit. It is felt that because of this approximation, the square-root limit overestimates the effect of gaseous radiation especially for physically thick boundary layers. The logarithmic approximation does not have this tendency; the prediction improves with the thickening of the boundary layer.

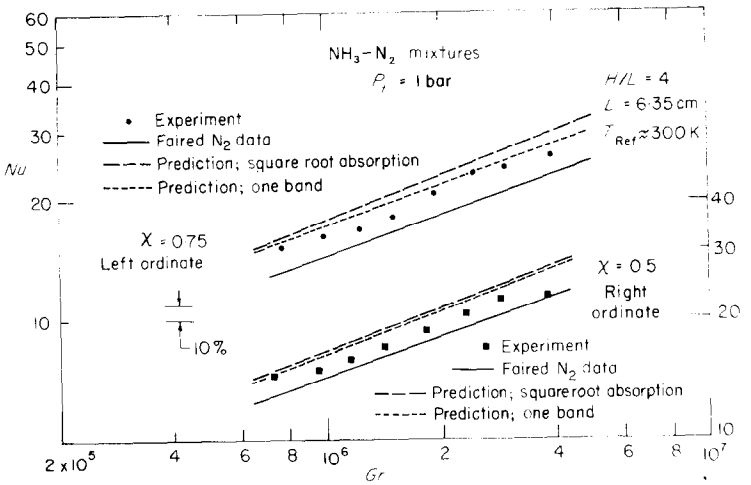

FIG. 14. Effect of radiation interaction for N_2–NH_3 mixtures; boundary layer regime, $P_t = 1$ bar.

Figures 12–14 present similar results for N_2–NH_3 mixtures at a total pressure of 1 and 2 bar. In general, the analysis overstimates in the influence of gaseous radiation. Again, a portion of this overestimation, especially for the 2 bar NH_3 mole fraction of 0·75 case, is due to being in the intermediate region between the square-root and logarithmic analyses. This intermediate region shifts towards higher total pressures as the mole fraction decreases [6]. Overall, the N_2–NH_3 results show greater discrepancies between analysis and experiment as the Grashof number increases. The agreement is excellent in Fig. 13 for the small mole fraction of NH_3; this, of course, is largely due to moving closer to pure free convection.

The speculation that the analysis based on square-root absorption limit overestimates the influence of gaseous radiation is somewhat supported by a comparison of the results given in [6] and [19]. Although, there is a difference between the two free convection problems reported in [6] and [19], the results of [19], which are not based on the assumption that one absorption region applies for the entire boundary layer, indicate that the decrease in interaction with decreasing pressure is much sharper than that indicated in [6].

In conclusion, it appears that the exponential wide-band model used with the assumptions invoked in [6] correctly predicts the magnitude and trends of radiation–convection at pressures where the band absorption in the boundary layer is primarily in the logarithmic limit. The agreement between theory and experiment at lower pressures (total pressure in the case of mixtures) is not as good; it is felt that this is primarily due to approximation of requiring the boundary to be entirely within the square-root absorption region or to the multi-dimensional nature of the enclosure problem rather than to the failure of the exponential band model. A two-dimensional numerical model of the entire enclosure problem is presently being developed. This model will include a radiation term formulated in terms of the zone method using the exponential wide-band model. This approach should give an estimate the multi-dimensional radiation effect.

REFERENCES

1. J. Gille and R. Goody, Convection in a radiating gas, *J. Fluid Mech.* **20**, 47 (1964).
2. W. P. Schimmel, J. L. Novotny and F. H. Olsofka, Interferometric study of radiation–conduction interaction, Proceedings of the Fourth Int. Heat Trans. Conf., paper R2.1. Elsevier, Amsterdam (1970).
3. J. L. Novotny and F. A. Olsofka, The influence of a non-absorbing gas in radiation-conduction interaction, *AIAA Prog. Astronautics Aeronautics* **24**, 410 (1971).
4. W. G. England and A. F. Emery, Thermal radiation effects on the laminar free convection boundary of an absorbing gas, *J. Heat Transfer* **91**, 37 (1969).
5. T. Audunson and B. Gebhart, An experimental and analytical study of natural convection with appreciable thermal radiation effects, *J. Fluid Mech.* **52**, 57 (1972).

6. J. C. Bratis and J. L. Novotny, Radiation interaction in real gases, *AIAA Prog. Astronautics & Aeronautics* **31** (1973).
7. E. R. G. Eckert and W. O. Carlson, Natural convection in an air layer enclosed between two vertical plates with different temperatures, *Int. J. Heat Mass Transfer* 2, 106 (1961).
8. J. W. Elder, Laminar free convection in a vertical slot, *J. Fluid Mech.* **23**, 77 (1965).
9. D. K. Edwards and W. A. Menard, Comparison of models for correlation of total band absorption, *Appl. Optics* **3**, 621 (1964).
10. W. P. Schimmel, Interferometric study of the interaction of gaseous radiation with conduction between parallel horizontal plates, Ph.D. Thesis, University of Notre Dame (1969).
11. W. L. Howes and D. R. Buchele, Practical considerations in specific applications of gas flow interferometry, NACA TN 3507 (1955).
12. *American Institute of Physics Handbook*, 2nd edition, McGraw-Hill, New York (1963).
13. S. Friberg, Ueber die Dispersion des Lichtes in gasformigen Koerpern innerhalb des ultravioletten Spectrums, *Z. Physik* **41**, 378 (1927).
14. J. C. Bratis, Interaction of gaseous radiation and natural convection heat transfer in an enclosed layer between two vertical parallel plates, Ph.D. Thesis, University of Notre Dame (1972).
15. A. E. Gill and A. Davey, Instabilities of a bouyancy driven system, *J. Fluid Mech.* **35**, 775 (1969).
16. W. P. Schimmel, J. L. Novotny and S. Kast, Effect of surface emittance and approximate kernels in radiation–conduction interactions, *Wärme- und Stoffübertragung* 3, 1 (1970).
17. C. L. Tien and J. E. Lowder, A correlation of total band absorptance of radiating gases, *Int. J. Heat Mass Transfer* **9**, 698 (1916).
18. E. R. G. Eckert and R. M. Drake, *Analysis of Heat and Mass Transfer*, McGraw-Hill, New York (1972).
19. J. L. Novotny, Radiation interaction in nongray boundary layers, *Int. J. Heat Mass Transfer* **11**, 1823 (1968).
20. R. E. Eichhorn, Natural convection in a thermally stratified fluid, *Progress in Heat Mass Transfer* Vol. 2, p. 41 (1969).
21. J. W. Elder, Numerical experiments with free convection in a vertical slot, *J. Fluid Mech.* **24**, 823 (1966).

INTERACTION RAYONNEMENT-CONVECTION EN REGIME DE COUCHE LIMITE DANS UNE ENCEINTE

Résumé—L'interaction du rayonnement thermique et de la convection libre en régime de couche limite pour une enceinte verticale est étudiée analytiquement et expérimentalement. On obtient par voie interférométrique les flux thermiques locaux issus de la paroi chauffée très réflectrice; la seconde paroi est une plaque refroidie assimilable à un corps noir. Les données expérimentales sont comparées à l'analyse type couche limite basée sur le modèle de large bande exponentielle. On présente des expériences faites pour NH_3 pur, N_2 pur et des mélanges N_2–NH_3 à des pressions atteignant 2 bar et à un niveau de température proche de 300 K.

WECHSELWIRKUNG VON STRAHLUNG UND KONVEKTION IM GRENZSCHICHTVERHALTEN EINES GESCHLOSSENEN BEHÄLTERS

Zusammenfassung—Die Wechselwirkung von Wärmestrahlung und freier Konvektion im Grenzschichtverhalten eines senkrechten, geschlossenen Behälters wird analytisch und experimentell untersucht. Der örtliche Wärmestrom an der hochreflektierenden, beheizten Wand im Behälter wird interferometrisch ermittelt; die zweite Wand ist eine fast schwarze, gekühlte Platte. Die Versuchsdaten werden verglichen mit einer Grenzschichtanalyse, die auf einem experimentellen Breitbandmodell aufbaut. Es werden Versuchsergebnisse aufgeführt für reines NH_3, reines N_2 und N_2—NH_3—Gemische für Drücke bis 2 bar bei einem Temperaturniveau nahe 300 K.

ВЗАИМОДЕЙСТВИЕ ИЗЛУЧЕНИЯ И КОНВЕКЦИИ В РЕЖИМЕ ПОГРАНИЧНОГО СЛОЯ В ПОЛОСТИ

Аннотация—Проведено теоретическое и экспериментальное исследование взаимодействия теплового излучения и свободной конвекции в пограничном слое в вертикальной полости. Локальные тепловые потоки от хорошо отражающей нагретой стенки полости находились интерферометрическим методом. Вторая стенка представляла из себя почти абсолютно черную охлаждаемую пластину. Экспериментальные данные сравниваются с решением уравнений типа пограничного слоя. Эксперименты проводились для чистого NH_3, чистого N_2 и смесей N_2–NH_3 для давлений до 2 бар при температуре около 300°K.